

# A Computer Vision-Based Quality Assessment Technique for the automatic control of consumables for analytical laboratories

Meriam Zribi

Università degli Studi Roma La Sapienza

Department of Basic and Applied Sciences for Engineering

Via Antonio Scarpa 14

Rome

Paolo Pagliuca

National Research Council

Institute of Cognitive Sciences and Technologies

Via Gian Domenico Romagnosi 18/A

Rome

Francesca Pitolli

Università degli Studi Roma La Sapienza

Department of Basic and Applied Sciences for Engineering

Via Antonio Scarpa 14

Rome

## Abstract

The rapid growth of the Industry 4.0 paradigm is increasing the pressure to develop effective automated monitoring systems. Artificial Intelligence (AI) is a convenient tool to improve the efficiency of industrial processes while reducing errors and waste. In fact, it allows the use of real-time data to increase the effectiveness of monitoring systems, minimize errors, make the production process more sustainable, and save costs. In this paper, a novel automatic monitoring system is proposed in the context of production process of plastic consumables used in analysis laboratories, with the aim to increase the effectiveness of the control process currently performed by a human operator. In particular, we considered the problem of classifying the presence or absence of a transparent anticoagulant substance inside test tubes. Specifically, a hand-designed deep network model is used and compared with some state-of-the-art models for its ability to categorize different images of vials that can be either filled with the anticoagulant or empty. Collected results indicate that the proposed approach is competitive with state-of-the-art models in terms of accu-

racy. Furthermore, we increased the complexity of the task by training the models on the ability to discriminate not only the presence or absence of the anticoagulant inside the vial, but also the size of the test tube. The analysis performed in the latter scenario confirms the competitiveness of our approach. Moreover, our model is remarkably superior in terms of its generalization ability and requires significantly fewer resources. These results suggest the possibility of successfully implementing such a model in the production process of a plastic consumables company.

**Keywords**— Automatic Monitoring, Green Economy, Industry 4.0, Deep Learning, Convolutional Neural Networks, Transfer Learning, Data Augmentation

## 1 Introduction

The pressures on the process industry to improve yields, reduce waste and increase profits make it essential to increase the efficiency of process operations [1]. In this respect, monitoring systems play a crucial role in making production processes efficient [2]. Unfortunately, traditional monitoring systems are increasingly unable to meet the highly dynamic and demanding requirements of today's industrial applications since they require the presence of various types of sensors (e.g., acoustic, electrical, magnetic, optical, thermal, ultrasonic or visual) [3,4] or service personnel. However, sensors are highly sensitive to noise perturbations and their accuracy is highly dependent on their calibration and the environmental conditions. In addition, the evaluation of human operators is subject to their expertise and physical (e.g., fatigue) and mental (e.g., stress) conditions.

One way to overcome these issues is to adopt the Industry 4.0 paradigm [5–7], which is growing exponentially [1]. Industry 4.0 means redefining processes, equipment and technologies in order to address challenges like sustainability, innovation, digital transformation, technological components and skills of the workers [8]. Specifically, Industry 4.0 requires companies to use smart sensors (“Sensor 4.0” [9–11]) and train skilled operators (“Operator 4.0” [12–14]). Successful examples of adopting the Industry 4.0 paradigm can be found in supply chain management [15,16], in the chemical industry [17,18] and in the food industry [19], although the lack of a common vision among companies still limits the diffusion of this approach [20,21].

To achieve the goals of Industry 4.0, one of the key elements is Artificial Intelligence (AI) [22–24]. Artificial Intelligence is indeed considered one of the key technologies for creating autonomous, collaborative production units with advanced capabilities for self-optimization and self-monitoring [6,25–27]. The aim is to use real-time data, analytics and AI techniques to improve production efficiency, flexibility and agility, and to develop new business models based on customized and sustainable production [22,28]. AI might also help mitigate pollution, a heavy social and environmental concern [29,30]. In fact, one possible countermeasure to reduce waste and preserve ecosystems is process automation [31]. Therefore, the use of AI approaches in industrial processes might play a key role. In [32–34] Convolutional Neural Network (CNN) models are employed to classify and automatically sort waste. Similar approaches exploiting deep learning for waste identification are those reported in [35,36]. In [37] the authors used deep transfer learning to detect waste in water.

The implementation of AI monitoring in the production process can dramatically reduce the waste of non-compliant components, enabling operators to intervene early during the manufacturing process to correct faulty operations. Ultimately, the goal is

to increase the accuracy of the quality control process and support the final decision making of the human expert, thereby reducing the cost of the process in terms of both wasted materials and time.

Among the AI techniques, Deep Learning (DL) [38] represents a widely used technique in process monitoring [39,40]. There are several examples in which deep networks have been successfully employed in such scenarios [41–47]. In [48] the authors used a deep CNN model to solve the problem of detecting smoke in normal and foggy environments. Specifically, they employed the VGG-16 deep network [49] combined with an attention mechanism attributing more importance to parts of the image containing smoke elements. In addition, they introduced a feature-level and decision-level module in order to extract more discriminative features enabling to distinguish between smoke and similar objects. A similar work is reported in [50]. In [51], a deep CNN is applied to address the problem of producing gravure cylinders in the printing industry.

In this paper, we present an automated AI system for monitoring the content of plastic vials, which was designed to meet a medical company's need to certify the quality of in vitro diagnostic devices. Currently, a human operator is responsible for this control, which consists of checking for the presence of a transparent anticoagulant in the test tubes. In addition, the inspection is limited to the external vials of each batch of the tubes produced: if the operator detects a defective vial, the entire batch is discarded, with inevitable disposal costs and high environmental impact. Overall, this control is not efficient and leads to numerous errors that make the tubes unusable. We propose an innovative monitoring system using Computer Vision (CV) to make the process efficient. CV systems are faster, more objective and can operate continuously to inspect thousands of vials per minute. They also provide more accurate inspection results than human operators when they are fine-tuned. By using CV systems, manufacturers can save costs and increase profits by reducing errors, improving yields and ensuring regulatory compliance [52].

The key idea behind the development of the proposed automatic certification system is to use a camera that allows the process to be monitored and certified by acquiring images at the critical steps of its execution. Specifically, we developed a new deep CNN model for the detection of the anticoagulant in the vials of an in vitro diagnostic device during the manufacturing process. We trained the proposed model for two different scenarios. In the first, the CNN is asked to detect the presence or the absence of the anticoagulant inside the vials, while in the second the model has to classify not only the presence or the absence of the anticoagulant but also the size of the vial. We compared our CNN model with state-of-the-art deep neural network architectures. Results of our analysis clearly show how the proposed approach is competitive with best models in the first scenario, while it is superior in the most complex scenario. Moreover, our model displays a better generalization capability, which turns out to be crucial for the development of efficient automatic monitoring systems. To our knowledge, the detection of nebulized chemicals within plastic laboratory instrumentation has not been previously addressed in the literature.

The remainder of the article is organized as follows: Section 2 contains a description of the considered monitoring system. The proposed model is introduced in Section 3. The experimental settings, the results we achieved and their analysis are presented in Section 4. Finally, in Section 5 we provide our conclusions and final remarks.

## 2 The Monitoring System

To make the process efficient and sustainable, the monitoring system must be embedded in the production line of the company performing the test tube analysis. The architecture of the system, shown in Fig. 1, consists of a metal frame attached to the floor on one side to give stability to the whole system. At the top of the structure there is a tunnel-shaped element, in which the transparent tubes containing the anticoagulant (Fig. 1, blue item) run. The structure is designed to shield the area in which the tubes are analyzed from ambient lighting, which could alter the results. The acquisition system, consisting of the acquisition board and the camera, is located in the false ceiling of the tunnel. The other two elements of interest highlighted in Fig. 1 are: the led card at the bottom (the green strip) illuminating the system and the photosensor responsible for sending the trigger for the acquisition of images (the orange item).

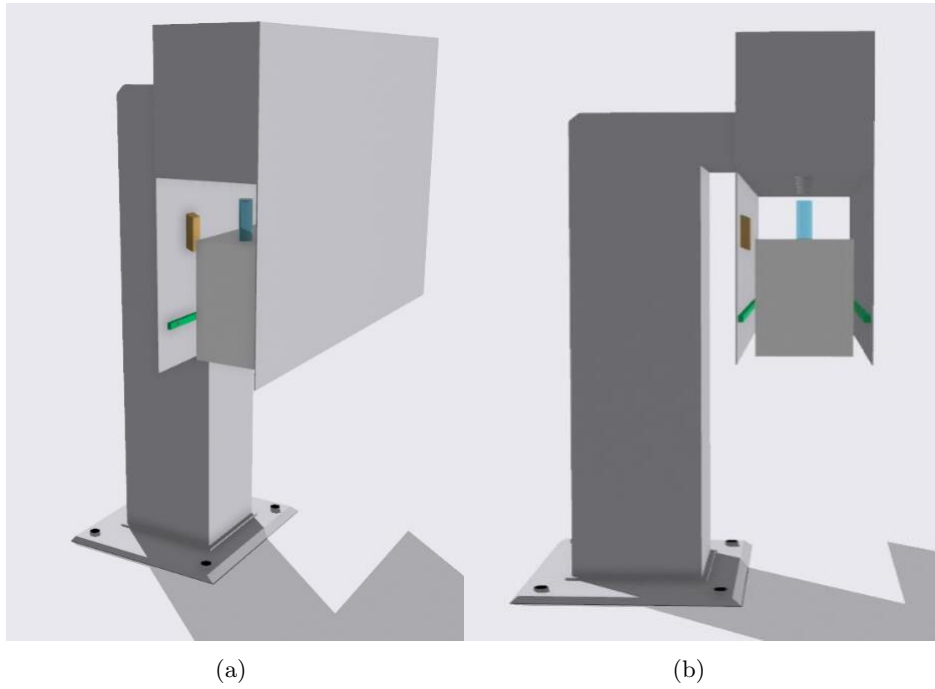


Figure 1: The monitoring system. Tubes (blue items) run within the tunnel. The system is illuminated by led cards (green items). A photosensor (orange item) gives the signal for the acquisition of the image.

Our goal is to detect the presence of the anticoagulant inside the test tubes that are placed inside white racks. The vials can be of different types and sizes and come with a label on the side wall. The anticoagulant may appear either as a droplet at the bottom of the tube, or as a spray on the side walls of the tube. Our tests have shown that the best setup for detecting the anticoagulant is the one in which the camera views the test tube from above since the presence of the label on the side walls limits

the size of the scene to be analyzed. An example of the vials to be checked is provided in Fig. 2. The configuration of the monitoring system we chose allows us to capture images as those shown in Fig. 3.



Figure 2: Example of analyzed test tubes. Vials have a label on the side wall. The unit of measurement is the milliliter. (**left**) a small vial (height: 10 cm, diameter: 1 cm, capacity: 6 ml); (**right**) a large vial (height: 10 cm, diameter: 1.3 cm, capacity: 9 ml).

### 3 Materials and Methods

We are interested in two different scenarios that may occur during the manufacturing process:

1. detecting the presence or the absence of the anticoagulant regardless of the size of the test tube (referred as  $2_{output-labels}$  case);
2. detecting the presence or the absence of the anticoagulant and the size (i.e., large or small) of the test tube (termed as  $4_{output-labels}$  case).

To address these challenges, two different strategies have been examined. The first is to create a CNN network from scratch [53], which is illustrated in the next section. The second is the transfer learning technique [54], which uses a pre-trained network and re-trains only the last layer with the data from the application of interest. We present the pre-trained deep network models we used in Section 4.2.

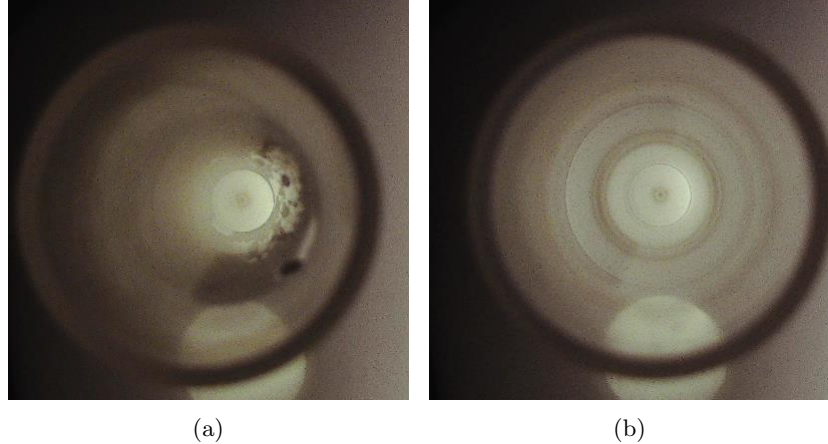


Figure 3: Images recorded by the camera. Left figure: a tube containing anti-coagulant. Right figure: an empty tube. Figure taken from [53].

### 3.1 The CNN model

In this section we describe the CNN model we designed, which proved to be effective in a preliminary study we conducted [53]. We will refer to this model as **ConvNet3\_4** since, as we will illustrate later, it consists of 3 convolutional layers and 4 fully-connected layers.

The whole monitoring process works as illustrated in Fig. 4, while the ConvNet3\_4 model is shown in Fig. 5. The model is organized in two main blocks:

1. **Feature extraction** block (*FEB*) consisting of a sequence of Convolutional Layers (CL);
2. **Classification** block (*CB*): it is a multi-layer fully-connected network that associates output labels to input data. The input of the classification block corresponds to the output of the feature extraction block.

#### 3.1.1 Feature Extraction Block (FEB)

The FEB is responsible for extracting relevant features from input images by convolution with a kernel function. To provide an explanation of the whole process, let us consider an input image represented as a tensor  $I$  of size  $m_1 \times m_2 \times m_c$ , where  $m_1$  denotes the height of the image,  $m_2$  indicates the width of the image and  $m_c$  represents the number of channels of the image. Suppose a filter (the kernel) is applied, which is described by a tensor  $K$  of size  $n_1 \times n_2 \times n_c$ , with  $n_c$  equal to  $m_c$ . The filter  $K$  is convolved with the image  $I$  resulting in a matrix  $F$  of size  $(m_1 - n_1 + 1) \times (m_2 - n_2 + 1) \times 1$ :

$$F[i, j] = (I * K)_{[i, j]} \quad (1)$$

Usually, a bias term  $b$  is added to the convoluted part  $F$  before an activation function  $\phi$  is applied:

$$Conv(I, K) = \phi((I * K) + b) \quad (2)$$

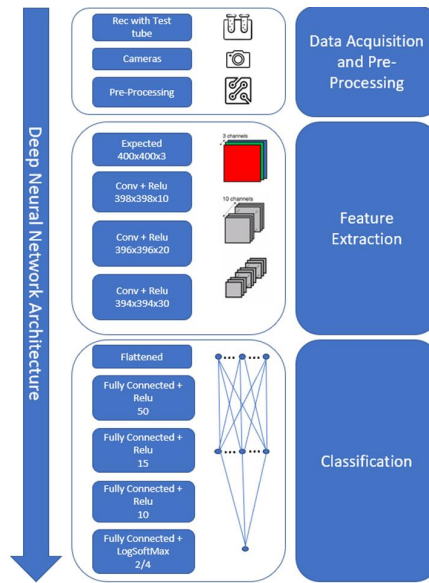


Figure 4: Deep Neural Network Architecture.

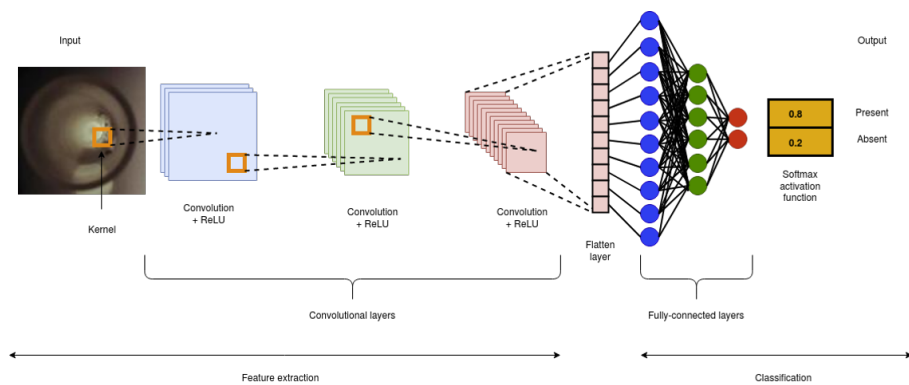


Figure 5: Illustration of the ConvNet3\_4 model.

This process is iterated for the number of convolutional layers in the model:

$$F_l = \text{Conv}(F_{l-1}, K) \quad l = 2, \dots, N_{\text{conv.layers}} \quad (3)$$

where  $N_{\text{conv.layers}}$  denotes the number of convolutional layers in the model and  $I = F_1$ .

Although not included in the ConvNet3\_4 model, in many cases a convolutional layer is followed by a pooling layer, which reduces the spatial size of the convoluted features and extracts the most relevant one [55]. However, we decided to avoid the use of pooling layers since experimental results (not shown) demonstrated that the technique does not provide any advantage in terms of accuracy. Conversely, the generalization capability of the model decreases. This implies that pooling has a negative impact on the performance of the model in the considered scenario.

Once the feature extraction is completed, the resultant  $F_{N_{\text{conv.layers}}}$  is flattened into a single vector  $x$  that will be the input of the CB.

### 3.1.2 Classification Block (CB)

The CB consists in a sequence of one or more fully-connected layers, each of which performs the following computation:

$$\begin{aligned} X &= w \times x + b \\ z &= \gamma(X) \end{aligned} \quad (4)$$

where  $\gamma$  is an activation function for the fully-connected layer. Also in this case, the process is repeated for the number of fully-connected layers in the model:

$$\begin{aligned} X_l &= w \times z_{l-1} + b \quad l = 2, \dots, N_{\text{fc.layers}} \\ z_l &= \gamma(X_l) \quad l = 2, \dots, N_{\text{fc.layers}} \end{aligned} \quad (5)$$

where  $N_{\text{fc.layers}}$  is the number of fully-connected layers. Once the process is terminated, the output of the last fully-connected layer indicates the probabilities that the input image belongs to each of the possible classes. In order to select among these options, the output passes through a function  $\psi$  (e.g., softmax as in the ConvNet3\_4 model or linear regression) to extract the more likely option, which represents the final model's output:

$$\hat{y} = \psi(z_{N_{\text{fc.layers}}}) \quad (6)$$

### 3.1.3 Backpropagation algorithm

The whole process we have just described allows a deep convolutional network like the ConvNet3\_4 model to predict an output  $\hat{y}$  for a given input image. However, in order to make the model learn the association between the input data (i.e., images) and the outputs (i.e., the labels), a backward process is required to adjust the model parameters so as to minimize the error between actual outputs and predictions. This is typically made by using the backpropagation algorithm [56]. We now provide an explanation of the method. Suppose we have a feed-forward network to be trained, which should associate the expected output  $y$  to a given input  $x$ . The network is usually initialized with random weights. Now, suppose the model produces the output  $\hat{y}$ , which

is different from the expected value  $y$ . We can compute the output error  $E = E(y, \hat{y})$  as a function of  $y$  and  $\hat{y}$ . Examples of error functions can be the Mean Squared Error or the Cross-Entropy Loss (the one used in this work). The backpropagation algorithm acts by adjusting the weights and biases of the neural network model in order to minimize the output error  $E$ . The backward process propagates from the output layer up to the first layer of the neural network model (CB in our case). The backpropagation algorithm works also for convolutional layers (FEB in the ConvNet3\_4 model). For further details, see [57].

To summarize, the proposed ConvNet3\_4 model first performs a forward pass to extract the relevant features from the input image and predicts the corresponding output (i.e., a label). Then, the error between the expected output and the model prediction is computed and a backward pass is run in order to adjust the model weights and attempt to minimize the error.

## 4 Results

In this section we describe the parameters of our model (Section 4.1) and the different pre-trained networks (Section 4.2) we used to perform our experiments, we illustrate the dataset used for training (Section 4.3) and we show the outcomes of our analyses (Sections 4.4 - 4.7).

### 4.1 Training phase

Table 1: Parameters of the FEB. For each convolutional layer (identified with the layer id), we report the number of input channels, the number of output channels, the kernel size and the stride. We also provide the size of input and output.

Layer id	# input channels	# output channels	Kernel size	Stride	# inputs	# outputs
1	3	10	3	1	$400 \times 400 \times 3$	$398 \times 398 \times 10$
2	10	20	3	1	$398 \times 398 \times 10$	$396 \times 396 \times 20$
3	20	30	3	1	$396 \times 396 \times 20$	$394 \times 394 \times 30$

The ConvNet3\_4 model has been trained on a dataset of RGB images having a resolution of  $400 \times 400$  pixels (see Section 4.3 for further details). Two examples of the input images are shown in Fig. 3.

The FEB consists of 3 convolutional layers: the first layer has a number of input channels corresponding to the RGB colors. For the other layers, we set:

$$n_{in-channels}(l) = n_{out-channels}(l-1) \quad l \geq 1 \quad (7)$$

where  $l$  is the layer identification number. The parameters of the FEB are listed in Table 1. The outputs of the last convolutional layer are used as inputs for the CB. It consists of 4 fully-connected layers (with identifiers numbered from 4 to 7), whose parameters are listed in Table 2. Last layer generates  $< n >_{output-labels}$  values, each one corresponding to a specific class. In order to select among the different outputs, we applied a softmax layer.

Table 2: Parameters of the CB. For each fully-connected layer (identified with the layer id), we report the number of inputs and the number of outputs.

Layer id	# of inputs	# of outputs
4	$394 \times 394 \times 30$	50
5	50	15
6	15	10
7	10	$< n >_{\text{output-labels}}$

In this work, we employed the Adam [58] optimizer with weight decay (set to  $10^{-2}$ ), i.e. a regularization technique penalizing large weights in order to keep the size of the network weights within limits. We chose the Adam optimizer since it represents a state-of-the-art optimizer in several DL domains [59–61]. Both the ConvNet3.4 and the deep networks described in Section 4.2 have been trained by using the parameters reported in Table 3. We used the same parameters for both the  $2_{\text{output-labels}}$  and the  $4_{\text{output-labels}}$  cases.

Table 3: List of parameters with values used for model’s training. The parameter  $\# \text{ of replications}$  refers only to the ConvNet3.4 model.

Parameter	Value
# of replications	10
# of epochs	50
learning rate	$10^{-4}$
batch size	64

## 4.2 Transfer learning

Transfer learning is defined as “the improvement of learning in a new task through the transfer of knowledge from a related task that has already been learned” [54]. Transfer learning is appealing since it allows to train a pre-trained model on new data without starting from scratch. Transfer learning has been successfully used in image classification. In [62] the authors applied transfer learning to the AlexNet [63], VGG-16 [49] and VGG-19 [49] networks. In [64] transfer learning is employed on the Inception v3 model [65]. In [66] the authors used pre-trained ResNet [67] and Inception networks to predict cell morphological changes due to chemical perturbations.

In our case, in the absence of similar applications, we studied the problem by assimilating it to more common applications in the literature, such as the detection of fog or smoke [48, 50]. We considered the following models:

- VGG-16 [49]
- VGG-19 [49]
- ResNet-50 [67]

- ResNet-152 [67]
- DenseNet-121 [68]
- DenseNet-201 [68]
- AlexNet [63]
- SqueezeNet1.1 [69]

Similarly to other applications using transfer learning techniques, the deep network models we used have been pre-trained on ImageNet [70] data set for image classification ( $14 \times 10^6$  images) in 1000 different categories. We then refined the original model, adjusting the last fully-connected layer from 1000 outputs to  $2_{output-labels}$  /  $4_{output-labels}$  classes to perform the expected classification regarding the presence or the absence of the anticoagulant and/or the type of the test tube.

### 4.3 Dataset

Thanks to the setup created in the laboratory, the training and test datasets were acquired by simulating an environment whose lighting was controlled (see Section 2). Under these conditions, 402 images were acquired (see the examples in Fig. 3). The dataset is composed as follows:

1. 101 images with large vial filled with anticoagulant
2. 100 images with large vial without the anticoagulant
3. 102 images with small vial full of anticoagulant
4. 99 images with small vial without the anticoagulant

All the images have a resolution of  $400 \times 400$  pixels. The dataset is balanced w.r.t. to the different output classes. Nevertheless, due to its extremely small size, the data augmentation technique [71] was applied. Data augmentation is crucial in DL processes, especially when only few data are available [72–76]. In fact, models trained on small datasets typically suffer from the overfitting issue [73, 77], i.e. they are effective at categorizing those data, but unable to generalize to new unseen inputs. Generalization is a paramount property that modern industrial processes must possess. Data augmentation has been largely used in image classification on available datasets, such as CIFAR-10 [78, 79] and MNIST [75]. In [80] the authors highlighted the benefit of applying data augmentation on CNNs compared to using regularization techniques, like weight decay [81] and dropout [82].

The list of transformations that have been applied to the original dataset is provided in Table 4. Overall, we applied 22 transformations to each image acquired in the laboratory. The final dataset is then composed of 9246 images. The training set consists of 7843 images (85%), while the test set includes 1403 images (15%). For more details about each transformation, its effect and the explanation of the parameters, the reader is referred to [83].

We want to stress that the dataset used in the two scenarios -  $2_{output-labels}$  and  $4_{output-labels}$  - is the same, the only difference is the labeling given to the images w.r.t. the specific experiment. In fact, there are two classifier outputs in the first condition ( $2_{output-labels}$  case), where the number of outputs is four in the second condition ( $4_{output-labels}$  case).

Table 4: List of transformations applied to increase the size of datasets used for training and test. Each transformation is applied to each image in the original dataset.

Type	# of transforms	Parameter
Rotation	5	random angle in range [30°, 150°]
Blur	3	random sigma in range [0.1, 5.0] kernel size = 5
Blur	3	random sigma in range [0.1, 5.0] kernel size = 9
Posterization	1	2 bits
Posterization	1	4 bits
Posterization	1	8 bits
Sharpness	1	sharpness_factor = 2
Inversion	1	
Solarization	1	threshold = 63
Solarization	1	threshold = 127
Solarization	1	threshold = 192
Equalization	1	
Horizontal flipping	1	
Vertical flipping	1	

#### 4.4 Cross-validation

Since the proposed ConvNet3\_4 model has been designed from scratch, we employed the cross-validation technique [84, 85] in order to verify whether our deep network is suitable for the considered monitoring problem. Moreover, cross-validation is a widely used tool to avoid overfitting to the input data [86–88]. Specifically, we adopted the  $k$ -fold cross-validation method [89, 90]. This technique partitions training data into  $k$  disjoint subsets, where the size of each subset is approximately the same: if we denote the number of training data as  $N_{tr\_data}$ , we can compute the size  $N_{tr\_subset}$  of each subset according to the following equation:

$$N_{tr\_subset} = \frac{(k-1) * N_{tr\_data}}{k} \quad (8)$$

An example of how  $k$ -fold cross-validation works is shown in Fig. 6: it takes the original training data as input and generates  $k$  different disjoint subsets, which are then used to evaluate the model.

It is worth noting that, as we stated above, this method allows to verify the suitability of a model for a specific problem. Indeed, at each iteration a new model is initialized and trained. Therefore, the technique returns  $k$  different models trained on distinct subsets. The overall accuracy of the model  $acc_k$  can be computed as:

$$acc_k = \frac{1}{k} \sum_{i=1}^k err_i \quad (9)$$

where  $err_i$  represents the classification error of the  $i$ -th fold.

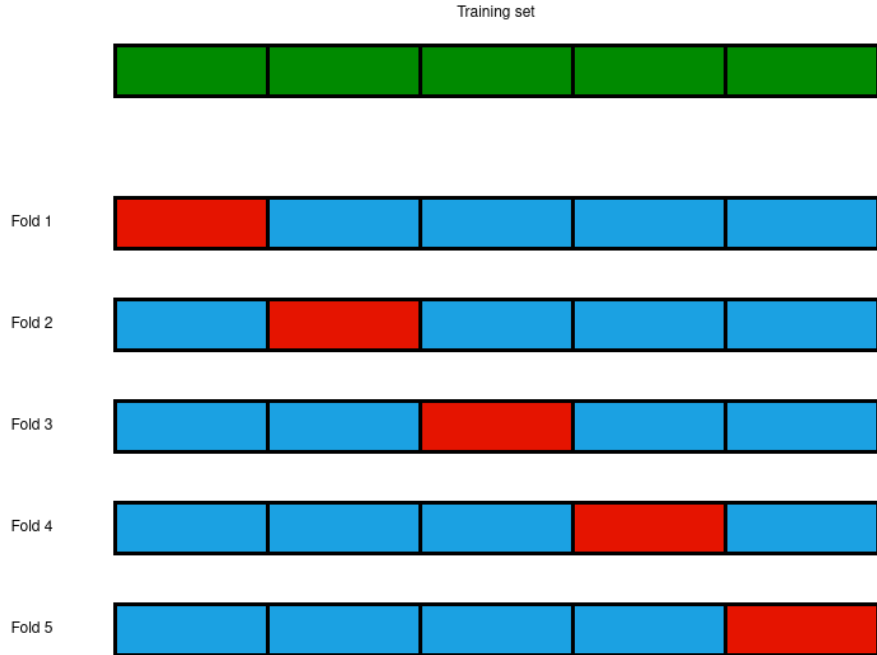


Figure 6: Illustration of the  $k$  – *fold* cross-validation method, with  $k = 5$ . At each iteration (i.e., the fold), part of the original training data (green in figure) is retained and used as validation set (red in figure). The remaining data (blue in figure) are used as training set for that specific model.

Table 5: Accuracy of each fold in the  $2_{output-labels}$  case.

<b>Fold 1</b>	<b>Fold 2</b>	<b>Fold 3</b>	<b>Fold 4</b>	<b>Fold 5</b>	<b>Average</b>
100%	99.946%	100%	99.946%	99.946%	99.968%

Table 6: Accuracy of each fold in the  $4_{output-labels}$  case.

<b>Fold 1</b>	<b>Fold 2</b>	<b>Fold 3</b>	<b>Fold 4</b>	<b>Fold 5</b>	<b>Average</b>
99.946%	96.322%	99.946%	100%	96.160%	98.475%

In this work we set  $k = 5$  as in Fig. 6. Tables 5 and 6 show the accuracy of the 5 different folds for the  $2_{\text{output-labels}}$  and the  $4_{\text{output-labels}}$  cases, respectively. Specifically, cross-validation gives an accuracy score above 98% in both conditions, which is a very good result. This confirms that the proposed ConvNet3\_4 model is suitable for the problem under consideration.

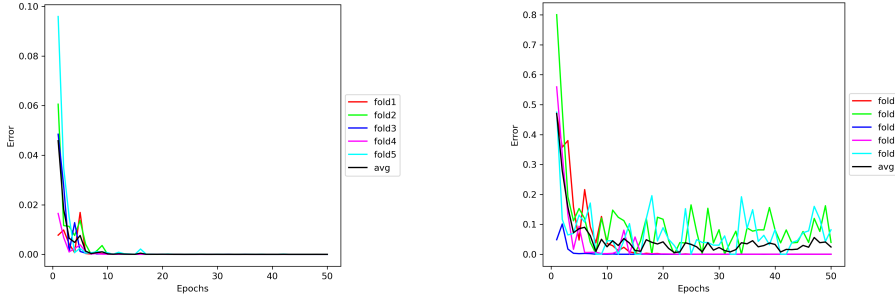


Figure 7: Training error during the  $k - \text{fold}$  cross-validation phase. Data refer to the best models returned by the procedure. Left:  $2_{\text{output-labels}}$  case. Right:  $4_{\text{output-labels}}$  case.

Fig. 7 shows the error curves when training the  $k$  different folds in the  $2_{\text{output-labels}}$  (Fig. 7, left) and the  $4_{\text{output-labels}}$  cases (Fig. 7, right). We chose the cross-entropy loss as an error metric. As can be observed, in the first case the error is significantly lower since the classification task is less complex (the error is around 0 after about 10 epochs). In the second case, however, the error curves have different trends depending on the particular fold and oscillations occur. This behavior is not surprising and is strictly dependent on the specific subset each fold has been evaluated with. In particular, because the subsets used in each fold are randomly extracted, it is possible that images are not equally balanced among the different classes.

#### 4.5 $2_{\text{output-labels}}$ case

In this section we present the results obtained in the  $2_{\text{output-labels}}$  case, which requires to distinguish between presence and absence of the anticoagulant inside vials.

##### 4.5.1 ConvNet3\_4 model

As we described in Section 4.1, we train the ConvNet3\_4 model 10 times, each time starting with different initial weights. This process allows us to minimize the impact of chance related to the extraction of random values. Moreover, repeating the training multiple times permits us to validate thoroughly our approach. At the end of the training process, we obtained an average accuracy of 99.551% on the test set in the  $2_{\text{output-labels}}$  case, i.e. a quasi-optimal performance. A detailed analysis of the classification capability of the best models trained for the  $2_{\text{output-labels}}$  case is provided in Fig. 8.

As can be observed, our best model successfully categorizes 1402 out of 1403 test images (Fig. 8, left). The AUC score is around 0.999 (Fig. 8, right), which represents an almost perfect classifier. This outcome is in agreement with those obtained

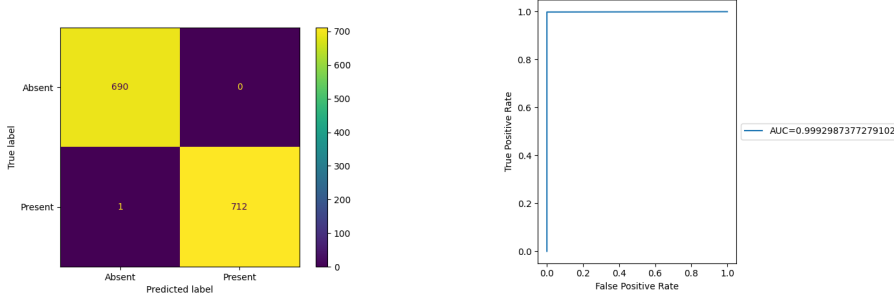


Figure 8: Classification results of our best model in the  $2_{output-labels}$  case. Data indicate the classification capability w.r.t. the images in the test set. Left: Confusion matrix. Right: ROC curve.

in [53], although the problem considered here represents a much more challenging task due to both the size of the training set and the complexity of the input images.

#### 4.5.2 Pre-trained models

Table 7 contains the outcomes obtained by the different models in the  $2_{output-labels}$  case. We computed five different metrics: accuracy, recall (or sensitivity), specificity, precision and F1-score.

As stated in Section 4.2, pre-trained models have been evaluated by using the weights for the training on the ImageNet dataset. To make the comparison fair, we kept the same settings (i.e., *# of epochs*, *learning rate* and *batch size*) listed in Table 3. Regarding the ConvNet3\_4 model, we consider the best model out of 10 replications of the experiment.

Table 7: Performance of the models in the  $2_{output-labels}$  case. We calculated the following metrics: accuracy (*Acc*), recall (*Rec*), specificity (*Spec*), precision (*Prec*) and F1-score (*F1*). All the metrics are bounded in the range  $[0, 1]$ . As far as the ConvNet3\_4 model is concerned, data refer to the best model out of 10 replications. The bold value indicates the best result we obtained.

Model	Acc	Rec	Spec	Prec	F1
ConvNet3_4	<b>0.9993</b>	0.9986	<b>1.0</b>	<b>1.0</b>	<b>0.9993</b>
VGG-16	0.9979	0.9986	0.9971	0.9972	0.9979
VGG-19	0.9979	0.9986	0.9971	0.9972	0.9979
ResNet-50	0.9765	0.9804	0.9725	0.9735	0.9769
ResNet-152	0.98	0.9762	0.9841	0.9844	0.9803
DenseNet-121	0.9979	0.9986	0.9971	0.9972	0.9979
DenseNet-201	0.9979	<b>1.0</b>	0.9957	0.9958	0.9979
AlexNet	0.9943	0.9986	0.9899	0.9903	0.9944
SqueezeNet1.1	0.4918	0.0	0.4918	0.0	0.0

As can be seen, all the models manage to achieve excellent results in terms of all the metrics with the exception of the SqueezeNet1.1 model, which classifies less than half of the images ( $Acc = 0.4918$ ). The sub-optimal performance of the latter model can be explained by considering that it classifies all the images according to only one of the two possible outputs (i.e., presence and absence of the anticoagulant).

To verify the capability of the trained models to generalize to new data, we run a post-validation phase on 4 different validation sets of increasing complexity. Some of them contain more than a single transformation. Specifically, for each validation set, we created 200 images for validation, obtained by applying 10 transformations to 20 images in the original dataset. We chose  $20 \div \langle n \rangle_{output-labels}$  images for each output class to create a uniformly distributed validation set as follows:

1.  $val\_set_1$ : obtained by applying the transformations listed in Table A1
2.  $val\_set_2$ : obtained by applying the transformations listed in Table A2
3.  $val\_set_3$ : obtained by applying the transformations listed in Table A3
4.  $val\_set_4$ : obtained by applying the transformations listed in Table A4

The results of the post-validation phase are shown in Fig. 9 and Table 8. For each dataset, we computed the validation error of each model. The outcomes show how the ConvNet3\_4 model significantly outperform the other pre-trained models (Kruskal-Wallis H test,  $p < 0.05$ ). In particular, our model obtains the lowest error in 3 out of 4 validation sets (see Table 8), which is a considerably good result. Regarding the pre-trained models, the VGG-16, VGG-19 and DenseNet-201 networks are competitive with the ConvNet3\_4 model. Conversely, the ResNet-50, ResNet-152, DenseNet-121, AlexNet and SqueezeNet1.1 are remarkably inferior to our model and fail in classifying images of the validation sets  $val\_set_1$  -  $val\_set_4$ .

Table 8: Validation error of the models in the  $2_{output-labels}$  case. As far as the ConvNet3\_4 is concerned, data refer to the best model. Bold values indicate the best results.

Model	$val\_set_1$	$val\_set_2$	$val\_set_3$	$val\_set_4$
ConvNet3_4	<b>0.0</b>	<b>0.0</b>	0.035	<b>0.05</b>
VGG-16	0.005	0.02	0.025	0.105
VGG-19	0.045	0.075	0.025	0.145
ResNet-50	0.5	0.5	0.5	0.5
ResNet-152	0.38	0.335	0.385	0.48
DenseNet-121	0.36	0.265	0.255	0.22
DenseNet-201	0.025	0.025	<b>0.02</b>	0.075
AlexNet	0.5	0.5	0.495	0.435
SqueezeNet1.1	0.5	0.5	0.5	0.5

An interesting outcome of this analysis is the discrepancy between categorization accuracy on the test set (results in Table 7) and the capability of classifying images on the validation sets (see Table 8) of some of the pre-trained deep networks (i.e., ResNet-50, ResNet-152, DenseNet-121 and AlexNet). In particular, these models exhibit poor performances even on the data in  $val\_set_1$ , which correspond to images that are more

likely to be acquired in the production process under consideration. This is partially surprising since the list of transformations in *val\_set<sub>1</sub>* (Table A1) can be seen as a subset of the transformations in Table 4. A possible explanation might be related to the overfitting issue: minimal changes in the input images make these models generate significant differences in the output predictions. Instead, the other pre-trained networks (i.e., VGG-16, VGG-19 and DenseNet-201) and the ConvNet3\_4 model are more robust to such perturbations.

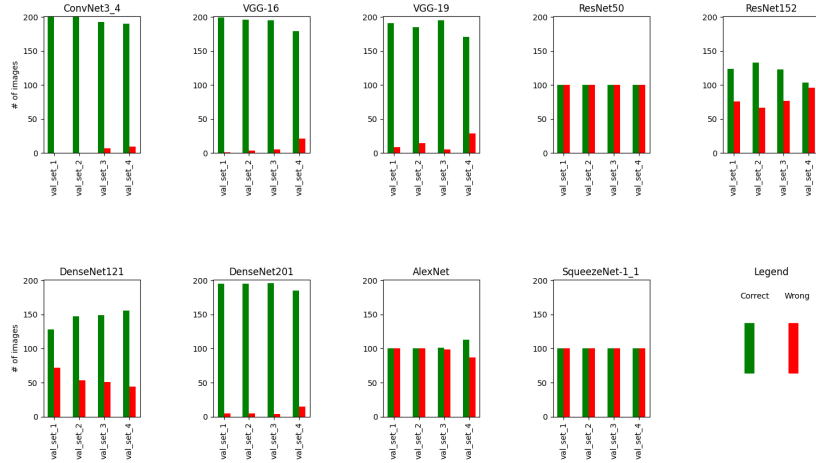


Figure 9: Post-validation bar plots for the  $2_{\text{output-labels}}$  case. As far as the ConvNet3\_4 is concerned, data refer to the best model.

## 4.6 $4_{\text{output-labels}}$ case

In this section we present the results achieved in the most complicated condition, i.e. the  $4_{\text{output-labels}}$  case, in which the model is required to distinguish both the presence or absence of the anticoagulant inside the test tube and the type of vial.

### 4.6.1 ConvNet3\_4

The ConvNet3\_4 model performed very well also in this challenging scenario. In fact, the average accuracy on the test set is 99.073%. The error curve of the ConvNet3\_4 model during training and test phases is shown in Fig. 10, left. The blue curve represents the classification error w.r.t. the images in the training set, while the red curve refers to the test set. As can be seen, the training error is around 0 at the end of the training. Conversely, starting at epoch 10, the test error stabilizes around a value of 0.05. The result is quite good considering the size of the training and test sets. The best model reached an accuracy level of 99.857%, i.e. a quasi optimal performance. Specifically, it correctly categorized 1401 out of 1403 test images (see Fig. 10, right), which is a remarkable result given the complexity of the problem.

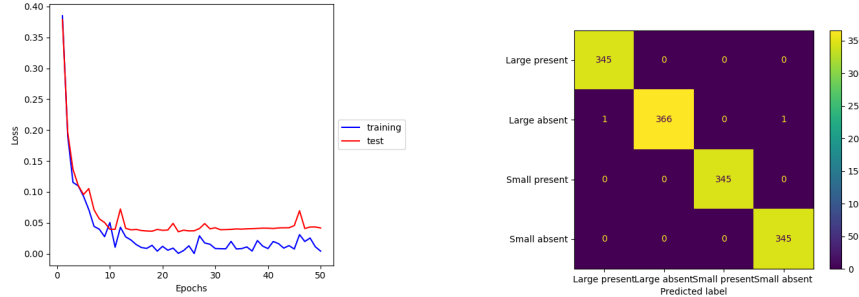


Figure 10: Results achieved by the ConvNet3\_4 model in the  $4_{output-labels}$  case. Left: error curve during training Data are obtained by averaging 10 replications of the experiment. Right: confusion matrix. Data refer to the classification capability of our best model with respect to the images in the test set.

Table 9: Performance of the models in the  $4_{output-labels}$  case. Because of the presence of four possible output classes, in this scenario we computed only the accuracy ( $Acc$ ) metric. As far as the ConvNet3\_4 model is concerned, data refer to the best model. Bold values indicate the best results we obtained.

Model	Acc
ConvNet3_4	<b>0.9986</b>
VGG-16	0.9922
VGG-19	0.9964
ResNet-50	0.8774
ResNet-152	0.881
DenseNet-121	0.99
DenseNet-201	0.9943
AlexNet	0.9922
SqueezeNet1.1	0.2459

#### 4.6.2 Pre-trained models

Similarly to the  $2_{output-labels}$  case, we analyzed the accuracy of the pre-trained models in this scenario. Results are provided in Table 9. As can be observed, there is a drop in performance due to the increased complexity of the classification task. This is more evident for the ResNet-50 and ResNet-152 models, whose performance goes below 0.9, and for the SqueezeNet1.1 network, which obtains a very low result of 0.2459 due to its tendency to classify all the images according to one output class.

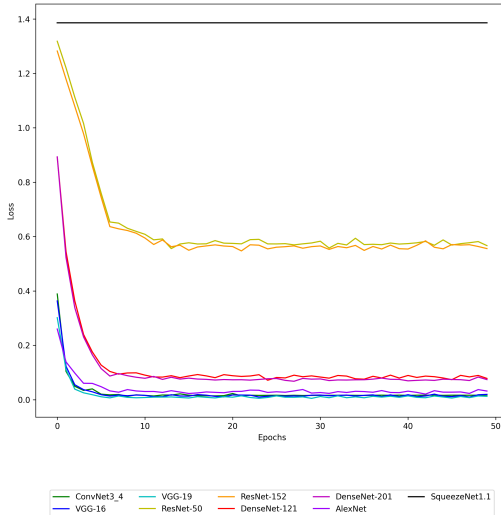


Figure 11: Error curves of the different models in the  $4_{output-labels}$  case. Data refer to the classification capability on the test set. Concerning the ConvNet3\_4 model, data refer to the best model.

The classification error of the models on the images of the test set is shown in Fig. 11. In particular, we can observe how the ConvNet3\_4 model and the pre-trained VGG-16, VGG-19 and AlexNet models quickly converge on a quasi-optimal performance (test error around 0.0). The SqueezeNet1.1 model does not improve its classification capability during the training. The ResNet-50 and ResNet-152 models soon reach an error of around 0.6, but they do not manage to further improve their accuracy. Finally, the DenseNet-121 and DenseNet-201 converge to a test error around 0.2.

Also in this case, we post-evaluated the capability of the trained models on the validation sets defined in Tables A1- A4. The results are provided in Table 10 and Fig. 12. As highlighted in Table 10, there is a remarkable fall in the classification capability of pre-trained networks. In fact, with the exception of DenseNet-201, the categorization error exceeds 0.5, that is these models are not able to correctly predict the output class for more than half of the images in the validation sets  $val\_set_1-val\_set_4$ . Specifically, the ResNet-50, ResNet-152, DenseNet-121, AlexNet and SqueezeNet1.1 models adopt a sub-optimal strategy consisting of associating each input image to one of the possible output classes. The VGG-16 and VGG-19 models implement a similar

Table 10: Validation error of the models in the  $4_{output-labels}$  case. As far as the ConvNet3\_4 is concerned, data refer to the best model. Bold values indicate the best results.

Model	<i>val_set<sub>1</sub></i>	<i>val_set<sub>2</sub></i>	<i>val_set<sub>3</sub></i>	<i>val_set<sub>4</sub></i>
ConvNet3_4	<b>0.01</b>	<b>0.025</b>	<b>0.105</b>	<b>0.07</b>
VGG-16	0.5	0.51	0.5	0.55
VGG-19	0.515	0.505	0.5	0.575
ResNet-50	0.735	0.75	0.75	0.745
ResNet-152	0.675	0.695	0.715	0.74
DenseNet-121	0.65	0.725	0.71	0.66
DenseNet-201	0.145	0.17	0.205	0.15
AlexNet	0.755	0.75	0.74	0.745
SqueezeNet1.1	0.75	0.75	0.75	0.75

strategy and return a prediction for the input image by selecting among two output classes. In addition, unlike the previous case, the categorization ability deteriorates immediately when dealing with the images in *val\_set<sub>1</sub>*. This means that these models do not generalize at all. Overall, the post-evaluation analysis clearly shows how the ConvNet3\_4 model is considerably better than others at generalizing to new unseen data (Kruskal-Wallis H test,  $p < 0.05$ ).

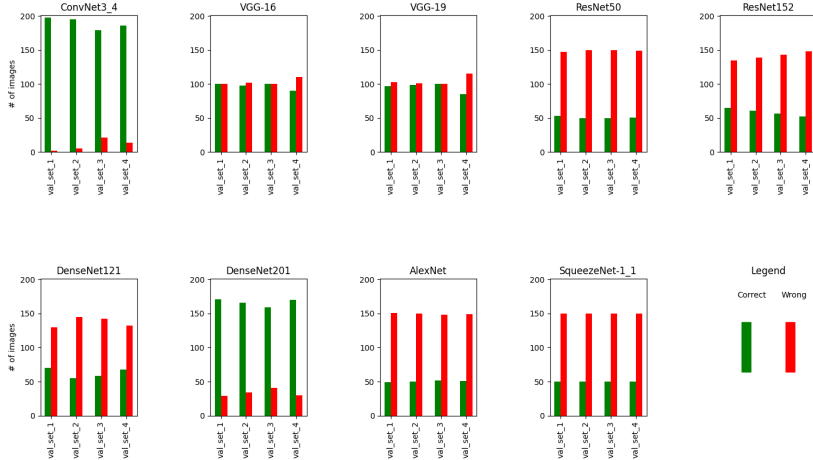


Figure 12: Post-validation bar plots for the  $4_{output-labels}$  case. As far as the ConvNet3\_4 is concerned, data refer to the best model.

## 4.7 Feature analysis

In this section we provide an analysis of the image features mainly impacting the model’s classification. We considered two different techniques for interpreting DL models: *Saliency* [91] and *Integrated Gradients* [92]. “Saliency” is a measure of which parts of the image contributed most to the target class prediction, and is represented by the “Saliency” map of the input image gradients w.r.t. the specified target class. Null saliency values represent regions of the image having no impact on the target class prediction, while positive saliency values indicate regions having a positive impact on the prediction [91]. Fig. 13 (center) represents the heat map of saliency of the input image shown in Fig. 13 (left). The color bar specifies the intensity of saliency, with white representing absence of saliency and blue indicating positive saliency, i.e. blue regions are most influential in deep learning model classification decision.

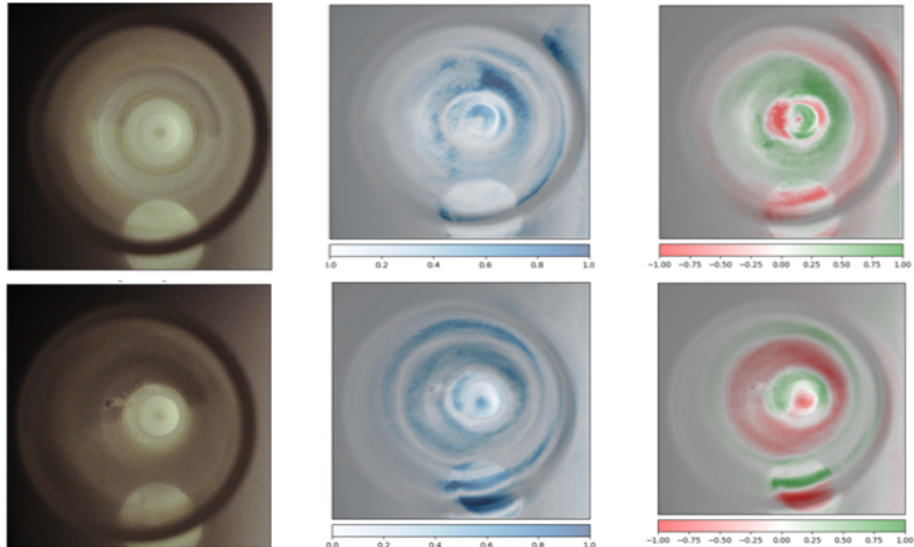


Figure 13: Comparison between raw image and feature maps. Images refer to the  $2_{\text{output-labels}}$  case. Top: big empty original image (left) and the corresponding *Saliency* (center) and *Integrated Gradients* (right) feature maps. Bottom: big filled original image (left) and the corresponding *Saliency* (center) and *Integrated Gradients* (right) feature maps.

The “Integrated Gradients” heat map represents the integrated attribution of each pixel to the model’s classification decision [92]. This heat map displays the regions of the image that most influenced the model’s classification decision by taking into account the entire input-output trajectory and the reference input distribution (base-lines) used in the attribution calculation. The “Integrated Gradients” heat map was generated by using the Integrated Gradients technique to calculate the importance of each pixel in the input image for the model prediction [92]. Positive values indicate that the corresponding pixels were deemed important. In the “Integrated Gradients” heat map shown in Fig. 13 (right), colors represent the degree to which each region of the image is predicted by the model. Red corresponds to negative attributions, while

green corresponds to positive attributions.

As can be observed, both the “Saliency” and the “Integrated Gradients” methods indicated how the central part of the input image is paramount for the model classification. However, our analysis reveals also an effect of the white circle in the bottom part of the images (Fig. 13, bottom center and bottom right figures), which corresponds to the space where a second vial could be inserted into the production process.

## 5 Conclusions

In this paper, we present an automated system that is able to monitor the presence or the absence of transparent anticoagulants. The goal is to integrate such a system into the production process of a company that handles plastic consumables to increase efficiency and reduce waste, in line with the Industry 4.0 paradigm. Specifically, we designed a deep network architecture, named ConvNet3\_4, for the ability to detect the presence or the absence of an anticoagulant in test tubes ( $2_{output-labels}$  case) and we performed a comparison with the state-of-the-art models. In a second experiment, we trained the models to classify not only the presence or the absence of the anticoagulant, but also the size of the vials ( $4_{output-labels}$  case). The results in Section 4 show that the proposed model is competitive with the best state-of-the-art models and superior in terms of generalization capability, i.e. the ability to correctly classify images previously not seen during training. This is also true for the more challenging  $4_{output-labels}$  case. Since industrial monitoring requires a high level of effectiveness, including a high degree of accuracy and the ability to work properly with new data, only the ConvNet3\_4 model demonstrates the performance level required for real industrial applications, while pre-trained networks drop dramatically in performance in the  $4_{output-labels}$  scenario. However, it is worth noting that the ConvNet3\_4 model has significantly more parameters than the pre-trained networks, which may improve their performance. We are planning to carry out a series of experiments in which we compare the models with the same number of parameters.

In the future, we plan to investigate other techniques to further improve both the classification performance of our model and the time required for training. A first issue we want to address is the minimization of the error fluctuations (see Fig. 10, left), which may depend on the diversities observed in the input images. One strategy to avoid this type of oscillations is to use adaptive weight decay [93, 94] during training, for example when there is an increase in the error value from one epoch to the next (see epochs 12 and 46 in Fig. 10, left). Furthermore, as we discussed in Section 4.7, the input images contain external components (i.e., the location of a second test tube) that affect the prediction of the model. The actual impact of such behavior has not been investigated in depth, although it is more likely to act as a random noise. Future work should be devoted to such analysis in order to improve the accuracy of the ConvNet3\_4 model and avoid bias. To this end, we are collecting a larger dataset in the laboratory, both to reduce the use of the data augmentation technique (Section 4.3) and to better assess the validity of our approach in a real-world monitoring scenario.

## Acknowledgments

The work of F.P. was partially supported by PNRR-CN1 SPOKE 6 Spoke 6 - Multi-scale modeling engineering applications B83C22002940006 under the MUR National Recovery and Resilience Plan funded by the European Union - NextGenerationEU.

## References

- [1] Morteza Ghobakhloo. Industry 4.0, digitization, and opportunities for sustainability. *Journal of cleaner production*, 252:119869, 2020.
- [2] Marco S Reis and Geert Gins. Industrial process monitoring in the Big Data/Industry 4.0 era: From detection, to diagnosis, to prognosis. *Processes*, 5(3):35, 2017.
- [3] Steven Y Liang, Rogelio L Hecker, and Robert G Landers. Machining process monitoring and control: the state-of-the-art. *J. Manuf. Sci. Eng.*, 126(2):297–310, 2004.
- [4] David M Scott. *Industrial process sensors*. CRC Press, 2018.
- [5] Henning Kagermann, Wolf-Dieter Lukas, and Wolfgang Wahlster. Industrie 4.0: Mit dem Internet der Dinge auf dem Weg zur 4. industriellen Revolution. *VDI nachrichten*, 13(1):2–3, 2011.
- [6] Henning Kagermann, Wolfgang Wahlster, Johannes Helbig, et al. Recommendations for implementing the strategic initiative INDUSTRIE 4.0. *Final report of the Industrie*, 4(0):82, 2013.
- [7] Elena G Popkova, Yulia V Ragulina, and Aleksei V Bogoviz. *Industry 4.0: Industrial revolution of the 21st century*, volume 169. Springer, 2019.
- [8] Mamad Mohamed. Challenges and benefits of Industry 4.0: An overview. *International Journal of Supply and Operations Management*, 5(3):256–265, 2018.
- [9] Mohd Javaid, Abid Haleem, Ravi Pratap Singh, Shanay Rab, and Rajiv Suman. Significance of sensors for Industry 4.0: Roles, Capabilities, and Applications. *Sensors International*, 2:100110, 2021.
- [10] Andrei Porokhnya and Ilia Yakimenko. Role of sensors in the paradigm of Industry 4.0. In *AIP Conference Proceedings*, volume 2911. AIP Publishing, 2023.
- [11] Andreas Schütze, Nikolai Helwig, and Tizian Schneider. Sensors 4.0–smart sensors and measurement technology enable Industry 4.0. *Journal of Sensors and Sensor systems*, 7(1):359–371, 2018.
- [12] David Romero, Johan Stahre, Thorsten Wuest, Ovidiu Noran, Peter Bernus, Åsa Fast-Berglund, and Dominic Gorecky. Towards an Operator 4.0 typology: a human-centric perspective on the fourth industrial revolution technologies. In *proceedings of the international conference on computers and industrial engineering (CIE46), Tianjin, China*, pages 29–31, 2016.
- [13] David Romero, Johan Stahre, and Marco Taisch. The Operator 4.0: Towards socially sustainable factories of the future, 2020.
- [14] Álvaro Segura, Helen V Diez, Iñigo Barandiaran, Ander Arbelaitz, Hugo Álvarez, Bruno Simões, Jorge Posada, Alejandro García-Alonso, and Ramón Ugarte. Visual computing technologies to support the Operator 4.0. *Computers & Industrial Engineering*, 139:105550, 2020.

- [15] Hajar Fatorachian and Hadi Kazemi. Impact of Industry 4.0 on supply chain performance. *Production Planning & Control*, 32(1):63–81, 2021.
- [16] Abhijeet Ghadge, Merve Er Kara, Hamid Moradlou, and Mohit Goswami. The impact of Industry 4.0 implementation on supply chains. *Journal of Manufacturing Technology Management*, 31(4):669–686, 2020.
- [17] Chasheng He, Chengwei Zhang, Tengfei Bian, Kaixuan Jiao, Weike Su, Ke-Jun Wu, and An Su. A Review on Artificial Intelligence Enabled Design, Synthesis, and Process Optimization of Chemical Products for Industry 4.0. *Processes*, 11(2):330, 2023.
- [18] Marco Vaccari, Riccardo Bacci di Capaci, Elisabetta Brunazzi, Leonardo Tognotti, Paolo Pierno, Roberto Vagheggi, and Gabriele Pannocchia. Optimally managing chemical plant operations: An example oriented by Industry 4.0 paradigms. *Industrial & Engineering Chemistry Research*, 60(21):7853–7867, 2021.
- [19] Abdo Hassoun, Abderrahmane Aït-Kaddour, Adnan M Abu-Mahfouz, Nikheel Bhojraj Rathod, Farah Bader, Francisco J Barba, Alessandra Biancolillo, Janna Cropotova, Charis M Galanakis, Anet Režek Jambrak, et al. The fourth industrial revolution in the food industry—Part I: Industry 4.0 technologies. *Critical Reviews in Food Science and Nutrition*, 63(23):6547–6563, 2023.
- [20] Sabai Khin and Daisy Mui Hung Kee. Factors influencing Industry 4.0 adoption. *Journal of Manufacturing Technology Management*, 33(3):448–467, 2022.
- [21] Zhanybek Suleiman, Sabit Shaikholla, Dinara Dikhanbayeva, Essam Shehab, and Ali Turkyilmaz. Industry 4.0: Clustering of concepts and characteristics. *Cogent Engineering*, 9(1):2034264, 2022.
- [22] Zohaib Jan, Farhad Ahamed, Wolfgang Mayer, Niki Patel, Georg Grossmann, Markus Stumptner, and Ana Kuusk. Artificial intelligence for Industry 4.0: Systematic review of applications, challenges, and opportunities. *Expert Systems with Applications*, 216:119456, 2023.
- [23] Varanon Uraikul, Christine W Chan, and Paitoon Tontiwachwuthikul. Artificial intelligence for monitoring and supervisory control of process systems. *Engineering applications of artificial intelligence*, 20(2):115–131, 2007.
- [24] Chunhui Zhao. Perspectives on nonstationary process monitoring in the era of industrial artificial intelligence. *Journal of Process Control*, 116:255–272, 2022.
- [25] László Monostori. Cyber-physical production systems: Roots, Expectations and R&D Challenges. *Procedia Cirp*, 17:9–13, 2014.
- [26] Birgit Vogel-Heuser, Christian Diedrich, Dorothea Pantförder, and Peter Göhner. Coupling heterogeneous production systems by a multi-agent based cyber-physical production system. In *2014 12th IEEE international conference on industrial informatics (INDIN)*, pages 713–719. IEEE, 2014.
- [27] Xuan Wu, Virginie Goepp, and Ali Siadat. Concept and engineering development of cyber physical production systems: a systematic literature review. *The International Journal of Advanced Manufacturing Technology*, 111:243–261, 2020.
- [28] Ricardo Silva Peres, Xiaodong Jia, Jay Lee, Keyi Sun, Armando Walter Colombo, and Jose Barata. Industrial artificial intelligence in Industry 4.0 - systematic review, challenges and outlook. *IEEE Access*, 8:220121–220139, 2020.

- [29] Christine W Chan and Guo H Huang. Artificial intelligence for management and control of pollution minimization and mitigation processes. *Engineering applications of artificial intelligence*, 16(2):75–90, 2003.
- [30] D Yadav, R Singh, A Kumar, and B Sarkar. Reduction of Pollution through Sustainable and Flexible Production by Controlling By-Products. *Journal of Environmental Informatics*, 40(2), 2022.
- [31] Paul N Cheremisinoff and Louise M Ferrante. *Waste reduction for pollution prevention*. Butterworth-Heinemann, 2013.
- [32] Mohammed Imran Basheer Ahmed, Raghad B Alotaibi, Rahaf A Al-Qahtani, Rahaf S Al-Qahtani, Sara S Al-Hetela, Khawla A Al-Matar, Noura K Al-Saqr, Atta Rahman, Linah Saraireh, Mustafa Youl dash, et al. Deep Learning Approach to Recyclable Products Classification: Towards Sustainable Waste Management. *Sustainability*, 15(14):11138, 2023.
- [33] Minh-Hieu Huynh, Phu-Thinh Pham-Hoai, Anh-Kiet Tran, and Thanh-Dat Nguyen. Automated waste sorting using convolutional neural network. In *2020 7th NAFOSTED Conference on Information and Computer Science (NICS)*, pages 102–107. IEEE, 2020.
- [34] Qiang Zhang, Xujuan Zhang, Xiaojun Mu, Zhihe Wang, Ran Tian, Xiangwen Wang, and Xueyan Liu. Recyclable waste image recognition based on deep learning. *Resources, Conservation and Recycling*, 171:105636, 2021.
- [35] Yash Narayan. DeepWaste: Applying deep learning to waste classification for a sustainable planet. *arXiv preprint arXiv:2101.05960*, 2021.
- [36] Nadish Ramsurrun, Geerish Suddul, Sandhya Armoogum, and Ravi Foogooa. Recyclable waste classification using computer vision and deep learning. In *2021 zooming innovation in consumer technologies conference (ZINC)*, pages 11–15. IEEE, 2021.
- [37] Harsh Panwar, PK Gupta, Mohammad Khubeb Siddiqui, Ruben Morales-Menendez, Prakhar Bhardwaj, Sudhansh Sharma, and Iqbal H Sarker. Aquavision: Automating the detection of waste in water bodies using deep transfer learning. *Case Studies in Chemical and Environmental Engineering*, 2:100026, 2020.
- [38] Yann LeCun, Yoshua Bengio, et al. Convolutional networks for images, speech, and time series. *The handbook of brain theory and neural networks*, 3361(10):1995, 1995.
- [39] Vahid Nasir and Farrokh Sassani. A review on deep learning in machining and tool monitoring: Methods, Opportunities, and Challenges. *The International Journal of Advanced Manufacturing Technology*, 115(9-10):2683–2709, 2021.
- [40] Rui Zhao, Ruqiang Yan, Zhenghua Chen, Kezhi Mao, Peng Wang, and Robert X Gao. Deep learning and its applications to machine health monitoring. *Mechanical Systems and Signal Processing*, 115:213–237, 2019.
- [41] Rahat Iqbal, Tomasz Maniak, Faiyaz Doctor, and Charalampos Karyotis. Fault detection and isolation in industrial processes using deep learning approaches. *IEEE Transactions on Industrial Informatics*, 15(5):3077–3084, 2019.
- [42] Ki Bum Lee, Sejune Cheon, and Chang Ouk Kim. A convolutional neural network for fault classification and diagnosis in semiconductor manufacturing processes. *IEEE Transactions on Semiconductor Manufacturing*, 30(2):135–142, 2017.

- [43] Yabin Liao, Ihab Ragai, Ziyun Huang, and Scott Kerner. Manufacturing process monitoring using time-frequency representation and transfer learning of deep neural networks. *Journal of Manufacturing Processes*, 68:231–248, 2021.
- [44] Yuting Lyu, Junghui Chen, and Zhihuan Song. Image-based process monitoring using deep belief networks. *IFAC-PapersOnLine*, 51(18):115–120, 2018.
- [45] Ke Mu, Lin Luo, Qiao Wang, and Fushun Mao. Industrial process monitoring and fault diagnosis based on temporal attention augmented deep network. *Journal of Information Processing Systems*, 17(2):242–252, 2021.
- [46] Hao Wu and Jinsong Zhao. Self-adaptive deep learning for multimode process monitoring. *Computers & chemical engineering*, 141:107024, 2020.
- [47] Jianbo Yu and Xuefeng Yan. Active features extracted by deep belief network for process monitoring. *ISA transactions*, 84:247–261, 2019.
- [48] Lijun He, Xiaoli Gong, Sirou Zhang, Liejun Wang, and Fan Li. Efficient attention based deep fusion CNN for smoke detection in fog environment. *Neurocomputing*, 434:224–238, 2021.
- [49] Karen Simonyan and Andrew Zisserman. Very deep convolutional networks for large-scale image recognition. *arXiv preprint arXiv:1409.1556*, 2014.
- [50] Salman Khan, Khan Muhammad, Shahid Mumtaz, Sung Wook Baik, and Victor Hugo C de Albuquerque. Energy-efficient deep CNN for smoke detection in foggy IoT environment. *IEEE Internet of Things Journal*, 6(6):9237–9245, 2019.
- [51] Javier Villalba-Diez, Daniel Schmidt, Roman Gevers, Joaquín Ordieres-Meré, Martin Buchwitz, and Wanja Wellbrock. Deep learning for industrial computer vision quality control in the printing Industry 4.0. *Sensors*, 19(18):3987, 2019.
- [52] Mohd Javaid, Abid Haleem, Ravi Pratap Singh, Shanay Rab, and Rajiv Suman. Exploring impact and features of machine vision for progressive Industry 4.0 culture. *Sensors International*, 3:100132, 2022.
- [53] Meriam Zribi, Paolo Pagliuca, and Francesca Pitolli. Convolutional neural networks for the automatic control of consumables for analytical laboratories. In *BUILD-IT2023 workshop*, pages 95–97. 2023.
- [54] Lisa Torrey and Jude Shavlik. Transfer learning. In *Handbook of research on machine learning applications and trends: algorithms, methods, and techniques*, pages 242–264. IGI global, 2010.
- [55] Ian Goodfellow, Yoshua Bengio, and Aaron Courville. *Deep learning*. MIT press, 2016.
- [56] David E Rumelhart, Geoffrey E Hinton, and Ronald J Williams. Learning representations by back-propagating errors. *nature*, 323(6088):533–536, 1986.
- [57] XueFei Zhou. Understanding the convolutional neural networks with gradient descent and backpropagation. In *Journal of Physics: Conference Series*, volume 1004, page 012028. IOP Publishing, 2018.
- [58] Diederik P Kingma and Jimmy Ba. Adam: A method for stochastic optimization. *arXiv preprint arXiv:1412.6980*, 2014.
- [59] Benoit Liquet, Sarat Moka, and Yoni Nazarathy. The mathematical engineering of deep learning, 2024.

- [60] Mohamed Reyad, Amany M Sarhan, and M Arafa. A modified Adam algorithm for deep neural network optimization. *Neural Computing and Applications*, pages 1–18, 2023.
- [61] Muhammad Yaqub, Jinchao Feng, M Sultan Zia, Kaleem Arshid, Kebin Jia, Zaka Ur Rehman, and Atif Mehmood. State-of-the-art CNN optimizer for brain tumor segmentation in magnetic resonance images. *Brain Sciences*, 10(7):427, 2020.
- [62] Manali Shaha and Meenakshi Pawar. Transfer learning for image classification. In *2018 second international conference on electronics, communication and aerospace technology (ICECA)*, pages 656–660. IEEE, 2018.
- [63] Alex Krizhevsky, Ilya Sutskever, and Geoffrey E Hinton. Imagenet classification with deep convolutional neural networks. *Advances in neural information processing systems*, 25, 2012.
- [64] Mahbub Hussain, Jordan J Bird, and Diego R Faria. A study on cnn transfer learning for image classification. In *Advances in Computational Intelligence Systems: Contributions Presented at the 18th UK Workshop on Computational Intelligence, September 5-7, 2018, Nottingham, UK*, pages 191–202. Springer, 2019.
- [65] Christian Szegedy, Vincent Vanhoucke, Sergey Ioffe, Jon Shlens, and Zbigniew Wojna. Rethinking the inception architecture for computer vision. In *Proceedings of the IEEE conference on computer vision and pattern recognition*, pages 2818–2826, 2016.
- [66] Alexander Kensi, Philip J Harrison, and Ola Spjuth. Transfer learning with deep convolutional neural networks for classifying cellular morphological changes. *SLAS Discovery: Advancing Life Sciences R&D*, 24(4):466–475, 2019.
- [67] Kaiming He, Xiangyu Zhang, Shaoqing Ren, and Jian Sun. Deep residual learning for image recognition. In *Proceedings of the IEEE conference on computer vision and pattern recognition*, pages 770–778, 2016.
- [68] Gao Huang, Zhuang Liu, Laurens Van Der Maaten, and Kilian Q Weinberger. Densely connected convolutional networks. In *Proceedings of the IEEE conference on computer vision and pattern recognition*, pages 4700–4708, 2017.
- [69] Forrest N Iandola, Song Han, Matthew W Moskewicz, Khalid Ashraf, William J Dally, and Kurt Keutzer. SqueezeNet: AlexNet-level accuracy with 50x fewer parameters and 0.5 MB model size. *arXiv preprint arXiv:1602.07360*, 2016.
- [70] Jia Deng, Wei Dong, Richard Socher, Li-Jia Li, Kai Li, and Li Fei-Fei. Imagenet: A large-scale hierarchical image database. In *2009 IEEE conference on computer vision and pattern recognition*, pages 248–255. Ieee, 2009.
- [71] Martin A Tanner and Wing Hung Wong. The calculation of posterior distributions by data augmentation. *Journal of the American statistical Association*, 82(398):528–540, 1987.
- [72] Agnieszka Mikolajczyk and Michał Grochowski. Data augmentation for improving deep learning in image classification problem. In *2018 international interdisciplinary PhD workshop (IIPhDW)*, pages 117–122. IEEE, 2018.
- [73] Connor Shorten and Taghi M Khoshgoftaar. A survey on image data augmentation for deep learning. *Journal of big data*, 6(1):1–48, 2019.

- [74] Luke Taylor and Geoff Nitschke. Improving deep learning with generic data augmentation. In *2018 IEEE symposium series on computational intelligence (SSCI)*, pages 1542–1547. IEEE, 2018.
- [75] Jason Wang, Luis Perez, et al. The effectiveness of data augmentation in image classification using deep learning. *Convolutional Neural Networks Vis. Recognit*, 11(2017):1–8, 2017.
- [76] Suorong Yang, Weikang Xiao, Mengcheng Zhang, Suhan Guo, Jian Zhao, and Furao Shen. Image data augmentation for deep learning: A survey. *arXiv preprint arXiv:2204.08610*, 2022.
- [77] Xue Ying. An overview of overfitting and its solutions. In *Journal of physics: Conference series*, volume 1168, page 022022. IOP Publishing, 2019.
- [78] Shanqing Gu, Manisha Pednekar, and Robert Slater. Improve image classification using data augmentation and neural networks. *SMU Data Science Review*, 2(2):1, 2019.
- [79] Cheng Lei, Benlin Hu, Dong Wang, Shu Zhang, and Zhenyu Chen. A preliminary study on data augmentation of deep learning for image classification. In *Proceedings of the 11th Asia-Pacific Symposium on Internetware*, pages 1–6, 2019.
- [80] Alex Hernández-García and Peter König. Further advantages of data augmentation on convolutional neural networks. In *Artificial Neural Networks and Machine Learning–ICANN 2018: 27th International Conference on Artificial Neural Networks, Rhodes, Greece, October 4–7, 2018, Proceedings, Part I 27*, pages 95–103. Springer, 2018.
- [81] Anders Krogh and John Hertz. A simple weight decay can improve generalization. *Advances in neural information processing systems*, 4, 1991.
- [82] Nitish Srivastava, Geoffrey Hinton, Alex Krizhevsky, Ilya Sutskever, and Ruslan Salakhutdinov. Dropout: a simple way to prevent neural networks from overfitting. *The journal of machine learning research*, 15(1):1929–1958, 2014.
- [83] [https://pytorch.org/vision/main/auto\\_examples/plot\\_transforms.html](https://pytorch.org/vision/main/auto_examples/plot_transforms.html).
- [84] Martin Anthony and Sean B Holden. Cross-validation for binary classification by real-valued functions: theoretical analysis. In *Proceedings of the eleventh annual conference on Computational learning theory*, pages 218–229, 1998.
- [85] Cullen Schaffer. Selecting a classification method by cross-validation. *Machine learning*, 13:135–143, 1993.
- [86] Sylvain Arlot and Alain Celisse. A survey of cross-validation procedures for model selection. 2010.
- [87] Benyamin Ghojogh and Mark Crowley. The theory behind overfitting, cross validation, regularization, bagging, and boosting: tutorial. *arXiv preprint arXiv:1905.12787*, 2019.
- [88] Luke A Yates, Zach Aandahl, Shane A Richards, and Barry W Brook. Cross validation for model selection: a review with examples from ecology. *Ecological Monographs*, 93(1):1557, 2023.
- [89] Thomas G Dietterich. Approximate statistical tests for comparing supervised classification learning algorithms. *Neural computation*, 10(7):1895–1923, 1998.
- [90] Isabelle Guyon, Amir Saffari, Gideon Dror, and Gavin Cawley. Model selection: beyond the bayesian/frequentist divide. *Journal of Machine Learning Research*, 11(1), 2010.

- [91] Karen Simonyan, Andrea Vedaldi, and Andrew Zisserman. Deep inside convolutional networks: Visualising image classification models and saliency maps. *arXiv preprint arXiv:1312.6034*, 2013.
- [92] Mukund Sundararajan, Ankur Taly, and Qiqi Yan. Axiomatic attribution for deep networks. In *International conference on machine learning*, pages 3319–3328. PMLR, 2017.
- [93] Amin Ghiasi, Ali Shafahi, and Reza Ardekani. Adaptive weight decay: On the fly weight decay tuning for improving robustness. *arXiv preprint arXiv:2210.00094*, 2022.
- [94] Kensuke Nakamura and Byung-Woo Hong. Adaptive weight decay for deep neural networks. *IEEE Access*, 7:118857–118865, 2019.

## A Validation sets

Table A1: List of transformations applied to generate the validation set  $val\_set_1$

Type	# of transforms	Parameter
Rotation	5	random angle in range $[210^\circ, 330^\circ]$
Blur	2	random sigma in range $[0.1, 5.0]$ kernel size = 5
Blur	2	random sigma in range $[0.1, 5.0]$ kernel size = 9
Posterization	1	6 bits

Table A2: List of transformations applied to generate the validation set  $val\_set_2$

Type	# of transforms	Parameter
Jitter	1	brightness = 0.0 contrast = 0.0 saturation = 0.0 hue = 0.0
Rotation + horizontal flipping	4	Rotation: random angle in range $[30^\circ, 330^\circ]$
Rotation + vertical flipping	4	Rotation: random angle in range $[30^\circ, 330^\circ]$
Autocontrast	1	

Table A3: List of transformations applied to generate the validation set  $val\_set_3$

Type	# of transforms	Parameter
Rotation	3	random angle in range $[5^\circ, 175^\circ]$
Rotation	3	random angle in range $[185^\circ, 355^\circ]$
Center crop + pad	1	Center crop: size = 300 Pad: size = 50 fill = 0
Center crop + pad	1	Center crop: size = 350 Pad: size = 25 fill = 0
Equalization + horizontal flipping	1	
Equalization + vertical flipping	1	

Table A4: List of transformations applied to generate the validation set  $val\_set_4$

Type	# of transforms	Parameter
Sharpness	1	sharpness_factor = 0.5
Sharpness	1	sharpness_factor = 1.5
Sharpness	1	sharpness_factor = 2.5
Sharpness	1	sharpness_factor = 3
Sharpness	1	sharpness_factor = 4
Inversion + horizontal flipping	1	
Inversion + vertical flipping	1	
Blur	3	random sigma in range $[0.1, 5.0]$ kernel size = 7